ADVANCES IN ATMOSPHERIC SCIENCES, VOL. 29, NO. 6, 2012, 1215–1226

A Study on the Dynamic Mechanism of the Formation of Mesoscale Vortex in Col Field

JIANG Yongqiang[1,2] (姜勇强), WANG Yuan*[1] (王 元), and HUANG Hong[1,2] (黄 泓)

[1] *Key Laboratory of Mesoscale Severe Weather/Ministry of Education of China, and School of Atmospheric Sciences, Nanjing University, Nanjing* 210093

[2] *Institute of Meteorology, PLA University of Science and Technology, Nanjing* 211101

(Received 10 October 2011; revised 11 April 2012)

ABSTRACT

The mesoscale vortex associated with a mesoscale low-level jet (mLLJ) usually causes heavy rainfall in the col field. The col field is defined as a region between two highs and two lows, with the isobaric surface similar to a col. Using a two-dimensional shallow water model, the meso-β scale vortex couplets (MβVCs) induced by eight types of mesoscale wind perturbations in an ideal col field were numerically simulated. With the sizes of ∼100 km, the MβVCs induced by northerly perturbation (NP) and southerly perturbation (SP) moved toward the col point. The sizes of MβVCs induced by southwesterly perturbation (SWP), southeasterly perturbation (SEP), northwesterly perturbation (NWP), and northeasterly perturbation (NEP) were relatively small for the perturbations moving toward dilatation axis. The MβVC induced by easterly perturbation (EP) and westerly perturbation (WP) could not develop because they quickly moved away from the col point, before the circulation could form. The size of the circulation was determined by the distance between the vortex and the col point. The closer to the col point the vortex was, the larger the size of vortex.

The comparisons of maximum vorticity and vorticity root mean square error (RMSE) of the NP, the SWP, and the WP show that the maximum vorticity and the vorticity RMSE of the NP decreased slower than other perturbations. Therefore, the weak environment of the col field favors the maintenance of vorticity and the formation of vortex. When a mesoscale vortex forms near the col point or moves toward the col point, it may maintain a quasi-stationary state in the stable col field.

Key words: col field, mesoscale vortex, mesoscale low-level jet, point vorticity, numerical simulation

Citation: Jiang, Y. Q., Y. Wang, and H. Huang, 2012: A study on the dynamic mechanism of the formation of mesoscale vortex in col field. *Adv. Atmos. Sci.*, **29**(6), 1215–1226, doi: 10.1007/s00376-012-1186-9.

1. Introduction

Many heavy rainfall events are related to mesoscale vortices with low-pressure centers. Some of these mesoscale vortices are mesoscale convective vortices (MCVs), identified by Johnston (1981). He used infrared satellite imagery to demonstrate that the MCVs exist in the 2.5–4.5-km layer above sea level. When sounding data from numerous cases was analyzed, results showed that the MCVs were favored by weak flow, weak vertical shear, weak background relative vorticity, and intense horizontal and vertical moisture gradients (Bartels and Maddox, 1991). These results further indicated that the rapid MCV generation observed can be explained by the stretching term of the vorticity equation. Many studies indicated that diabatic heating plays a central role in the intensification and maintenance of the MCV (Rutledge and Houze, 1987; Raymond and Jiang, 1990; Hertenstein and Schubert, 1991; Chen and Frank, 1993; Fritsch et al., 1994; Davis and Weisman, 1994; Jiang and Raymond, 1995; Houze, 2004).

In addition to the MCVs, many low-level mesoscale vortices are able to cause heavy rainfall. Some of them form in the col (or saddle) field and within the low-level shear line in the mid-latitude of East Asia. The

*Corresponding author: WANG Yuan, yuanasm@nju.edu.cn

col field is defined as a region between two highs and two lows, with the isobaric surface similar to a col. The famous "98.7" torrential rainfall event which occurred in July 1998 over eastern Hubei Province was caused by a series of mesoscale vortices in a stable col field (Hu et al., 2001; Bei et al., 2002; Xu and Gao, 2002; Chen and Feng, 2003). Some other studies (Zhang and Fritsch, 1988; Chen et al., 2007; Jiang and Wang, 2010) also found that the col fields favor the onset of heavy rainfall.

The close relationship between heavy rainfall and a low-level jet (LLJ) has been reported in many studies (e.g., Akiyama, 1973a, b; Matsumoto, 1973; Ninomiya and Akiyama, 1974; Tao, 1980; Chen, 1982, 1983; Chen and Yu, 1988; Arritt et al., 1997; Li et al., 1997; Chen and Hsu, 1997; Chen et al., 2005, 2006; Wang and Gao, 2006; Zhai et al., 2007; Chu and Tan, 2010; Sun et al., 2010; Xu et al., 2011). Ray (1986) defined the LLJ as a strong and narrow quasi-horizontal flow that has a strong vertical wind shear. It is well known that the LLJ features supergeostrophic wind that provided low-level warm and moist air which causes potential unstable stratification and upward motion. There is a positive vorticity region to the left and a convergence region at the foreside of the LLJ axis. Some perturbations usually form near the LLJ and spread along the LLJ axis. The sudden increase of wind velocity along the LLJ axis, called wind velocity fluctuation, may lead to intense precipitation. The numerical simulation performed by Chen et al. (1998) indicates that a mesoscale LLJ (mLLJ) is responsible for the rainstorm along the mei-yu front in the Changjiang-Huaihe Basin, eastern China on 12–13 June 1991. The mLLJ develops simultaneously with the rainstorm, and therefore positive feedback occurs between the mLLJ and the rainstorm.

The heavy rainfall triggered by mesoscale vortex in the col field is usually correlated with a mLLJ. Due to the lack of available temporal and spatial observation data with high resolution, the mLLJ is rarely observed in conventional meteorological sounding network during heavy rainfall. However, it can be found with intensive observations and in mesoscale numerical simulations. The numerical simulation related to the "98.7" torrential rainfall event over eastern Hubei Province presented by Jiang and Wang (2010) suggested that a large-scale LLJ existed to the south of the stable col field, while the mesolow and the associated heavy rainfall were caused by the mLLJ on the south side of the intense precipitation region. There is a close relationship between strong precipitation, the mLLJ, and the mesolow. Using a mesoscale Eta-coordinate model, the extremely heavy rainfall event over Shanghai on 6 July 2001 was numerically simulated (Jiang et al., 2004). The intense rainfall occurred in a col field when the mesolow developed in association with a strengthened mLLJ. Although these studies have indicated that col fields favor the formation of mesolows, the reasons for the formation of the mesolow and the mLLJ are not yet clear.

In this study, a shallow water model is employed to simulate the evolution of a dynamical vortex in a col field under the influence of different wind perturbations, and the possible dynamic formation mechanism of the mesoscale vortex is discussed. Section 2 briefly describes the shallow water model and the initial fields. Section 3 gives the numerical simulated results and some discussion, and conclusions are given in the last section.

2. Shallow water model and initial fields

2.1 *Model description*

A shallow water model was developed by Gerhard Erbes in Stockholm University of Sweden (Erbes, 1992, 1993). The model uses two-dimensional flux form, inviscid and non-stratified approximation. It satisfies mass and momentum conversation, and the discontinuity phenomenon has been properly eliminated. The centered spatial difference scheme and the leapfrog temporal scheme with Asselin filter and radiation boundary conditions are used in this model. In Cartesian coordinates, the equations can be written as

$$\frac{\partial(uh)}{\partial t}+\frac{\partial(u^2h+gh^2/2)}{\partial x}+\frac{\partial(vuh)}{\partial y}$$
$$=-gh\frac{\partial h_{\mathrm{T}}}{\partial x}+fvh+K\nabla^2(uh)\,, \tag{1}$$
$$\frac{\partial(vh)}{\partial t}+\frac{\partial(uvh)}{\partial x}+\frac{\partial(v^2h+gh^2/2)}{\partial y}$$
$$=-gh\frac{\partial h_{\mathrm{T}}}{\partial y}-fuh+K\nabla^2(vh)\,, \tag{2}$$
$$\frac{\partial h}{\partial t}+\frac{\partial(uh)}{\partial x}+\frac{\partial(vh)}{\partial y}=K\nabla^2(h)\,, \tag{3}$$

where u and v are the x- and y-components of the wind, respectively, h is the height of the free surface of the fluid, h_{T} is the terrain height, K is the diffusion coefficient, g is the gravitational constant, f is the Coriolis parameter, and ∇^2 is the horizontal Laplacian operator.

The resolution of the horizontal grid is 10 km. The computational grid point is 601×601. The model was run for 48 h. In this study it is assumed that the Coriolis parameter f is a constant (the mid-latitude f-plane assumption), i.e., $f_0=1.26\times10^{-4}$ s^{-1}.

2.2 *Initial fields*

The initial fields of the model include a col field as background and wind perturbations. Petterssen (1956) indicated that a two-dimensional linear wind field could be expressed as a combination of translation, divergence, deformation, and vorticity components:

$$\bar{u} = u_0 + ax + bx - cy \,, \tag{4a}$$

$$\bar{v} = v_0 - ay + bx + cx \,, \tag{4b}$$

where the coefficients a, b, and c are deformation, dilatation-contraction and rotation coefficient, respectively, and all are constants. The bar "$^-$" denotes background. For simplicity, the col field is expressed by deformation terms:

$$\bar{u} = ax \,, \tag{5a}$$

$$\bar{v} = -ay \,. \tag{5b}$$

When the background wind field is given, the background geopotential height $\bar{h}$ can be obtained using the geostrophic winds balance:

$$\bar{u} = -\frac{g}{f}\frac{\partial \bar{h}}{\partial y} \,, \tag{6a}$$

$$\bar{v} = \frac{g}{f}\frac{\partial \bar{h}}{\partial x} \,. \tag{6b}$$

With Eqs. (5a) and (5b), $\bar{h}$ can be obtained by integrating Eqs. (6a) and (6b)

$$\bar{h} = -\frac{fa}{g}xy + A, \tag{7}$$

where A is a constant. Thus, the winds and geopotential heights of all grid points can be calculated using Eqs. (5a), (5b), and (7). In this study, $a = 0.05$ and $A = 3000$ gpm. It was assumed that $x_0 = y_0$=0 at the col point.

Figure 1a gives wind vectors and geopotential heights of the col field. In this study, eight types of wind perturbations were considered to simulate the different mLLJs: such as northerly perturbation (NP), southerly perturbation (SP), southwesterly perturbation (SWP), northwesterly perturbation (NWP), southeasterly perturbation (SEP), northeasterly perturbation (NEP), easterly perturbation (EP) and westerly perturbation (WP). The wind speed of the perturbation was calculated as follows:

$$u' = U_0 e^{-cr^2} \,, \tag{8a}$$

$$v' = V_0 e^{-cr^2} \,, \tag{8b}$$

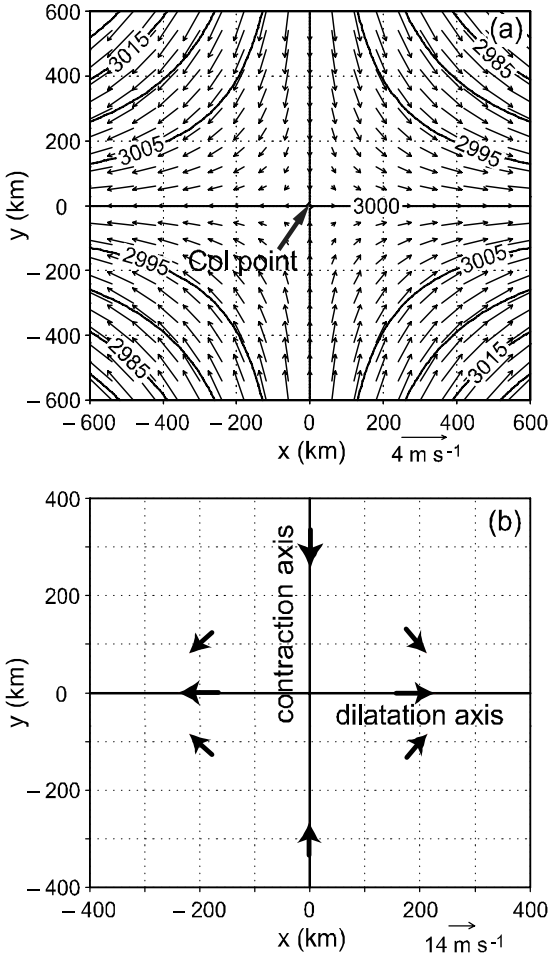

Fig. 1. Initial col field and wind perturbations. (a) Initial winds and geopotential height in col field with pure deformation. The vectors denote wind (units: m s^{-1}) and lines are geopotential height (units: gpm), (b) The schematic diagram of wind perturbations, the arrows denote the center wind of the perturbation (units: m s^{-1}).

where U_0, V_0 is the maximum x- and y-component of wind speeds at the center of perturbation respectively. r is the distance apart from the perturbation center, c is the attenuation coefficient of the wind speed which is set as a constant of 0.15, and the maximum wind speed of perturbation center is set as 14 m s^{-1}. Figure 1b shows the schematic diagram of meso-β scale wind perturbations and dilatation and contraction axes.

To balance the initial perturbation winds, the perturbation geopotential height h' was calculated using the geostrophic wind constraint:

$$u' = -g\partial h'/f\partial y \,, \tag{9a}$$

$$v' = g\partial h'/f\partial x \,, \tag{9b}$$

where u' and v' are the components of the wind perturbation. Differentiating Eqs. (9a) and (9b) yields

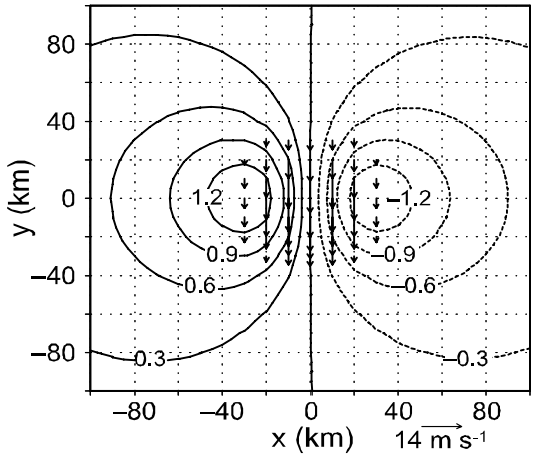

Fig. 2. Initial NP (arrows, units: m s^{-1}) and the balanced geopotential height (lines, units: gpm).

$$\nabla^2 h' = f\zeta'/g\,, \tag{10}$$

where ζ' is the relative vorticity perturbation (for convenience, the vertical component of the relative vorticity vector is called as vorticity), and $\zeta' = \partial v'/\partial x - \partial u'/\partial y$. Equation (10) is a Poisson equation. Given proper boundary conditions and initial wind fields, the h' can be calculated with the successive over-relaxation iterative method (SOR). Figure 2 shows the initial NP and the balanced geopotential height.

3. Numerical simulations

3.1 *NP and SP*

Figure 3 shows the evolution of simulated stream and vorticity fields induced by NP at the axis of contraction. At the beginning of integration, the meso-β scale perturbation, which is ∼300 km apart from the col point, produced a pair of mesoscale point-like vorticities (i.e., the size of the vorticity perturbation is so small that it can be regarded as a point vorticity). The positive vorticity was located to the east side of contraction axis, with the maximum value $> 30\times10^{-5}$ s^{-1}, and the negative vorticity was located to the west (Fig. 3a). At t=1 h, there were clear cyclonic and anticyclonic curves at the vorticity centers (not shown). The vorticity couplet moved southward toward the col point, ∼200 km apart from the col point at t=10 h, and a meso-β scale vortex couplet (MβVC) formed at t=14 h (not shown). The closer to the col point the MβVC became, the more slowly the MβVC moved. By t = 36 h, the MβVC was ∼80 km apart from the col point, with a size of vortex ∼100 km. However, the vorticity in the vortex center decreased to 15×10^{-5} s^{-1} (Fig. 3b). When the MβVC was close to the col point, it moved so slowly that it appeared to be quasi-stationary. Although the intensity of vorticity gradually decreased, the size of vortex remained ∼100 km.

The simulated stream and vorticity fields of SP were similar to that of NP. At the initial time, the positive and negative vorticities were located to the west and east side of the contraction axis, respectively (not shown). The size of vortex was also ∼100 km when the MβVC moved close to the col point at t = 36 h (Fig. 3c). The results of the simulation indicate that the col field favors the development of meso-β scale vortex (MβV).

The simulations of NP and SP show that the weak MβVC induced by perturbation moved slowly along the axis of contraction and developed rapidly as it approached the col point with the circulation sizes ∼100 km.

3.2 *SWP*

To investigate whether the MβVC can develop well when it moves along the dilatation axis in the col field, simulations with SWP, SEP, NWP and NEP are performed.

At the initial time, the SWP was located to the south of dilatation axis (not shown). The SWP moved toward the dilatation axis, under the effect of the southwesterly, and induced an MβVC, with the size of vortex ∼50 km at t = 1 h (not shown). The anticyclonic circulation was weaker than the cyclonic circulation; the former was farther from the col point. The MβVC moved northeastward and reached the south side of dilatation axis at t=10 h, with the maximum positive vorticity decreasing to $< 25\times10^{-5}$ s^{-1} (Fig. 3d). From then on, the MβVC became weaker and weaker as it is moved away from the col point. The circulations dissipated by t=30 h. The results indicate that the dilatation axis was also a favorable background for the development of MβVC, but the size of the vortex located at the dilatation axis was smaller than that at the col point.

3.3 *Other perturbations*

In the experiments of NWP, NEP and SEP, the simulated vortices were similar to that of the SWP (Figs. 4a–c). The circulation close to the col point was also stronger than that far from the col point.

In the EP and WP experiments, the induced weak MβVCs weakened and quickly dissipated while they moved away from the col point along the dilatation axis. Even in the vicinity of vorticity centers, the streamlines had a small curve. There was not enough time to form circulations. The simulated stream and vorticity fields at t=10 h are shown in Fig. 4d.

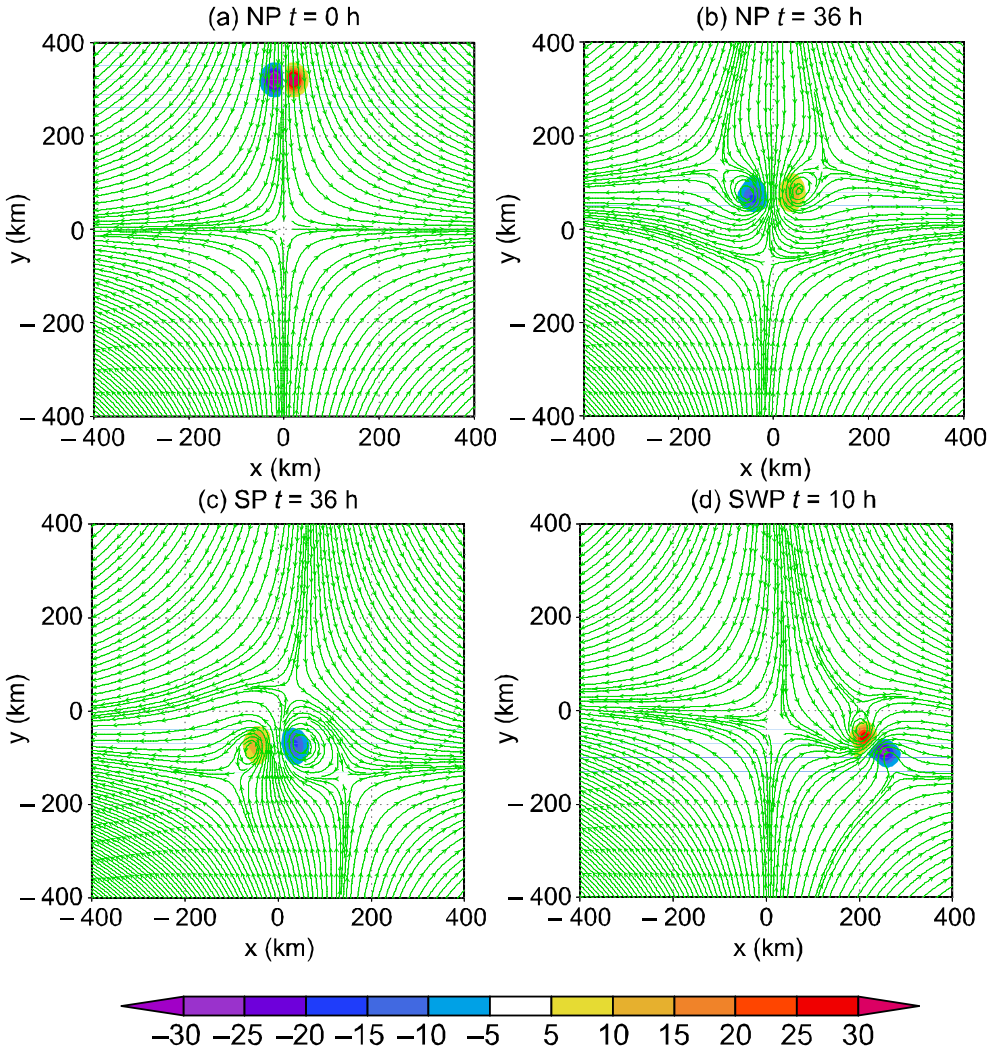

Fig. 3. Evolution of simulated stream and vorticity fields induced by wind perturbations. (a) NP at t=0 h, (b) NP at t=36 h, (c) SP at t=36 h, and (d) SWP at t=10 h. The shadings denote vorticity (units: 10^{-5} s^{-1}).

3.4 *Analyses of the kinetic energy, maximum vorticity and RMSE*

To quantify the differences of the different perturbations, we defined the total kinetic energy (E_k) per unit mass as

$$E_k = \sum \frac{1}{2}\left(u_{ij}^2 + v_{ij}^2\right), \tag{11}$$

where i and j run over x and y grid points over 700 km×700 km, with the center at the initial col point. Because the evolutions of E_k of SP and EP were similar to that of NP and WP, respectively, and the evolutions of E_k of the SEP, NEP and NWP were similar to that of SWP, it was only necessary to calculate the E_k values of NP, SWP, and WP.

Figure 5a shows the evolution of E_k/E_{k0} (E_{k0} is the initial E_k) in the grid of different perturbations. The E_k/E_{k0} of all the perturbations exhibited similar tendencies. The E_k/E_{k0} increased from 1.0 to ~1.6 at t=6 h, then it decreased to ~0.8 at t=11 h. After t=11 h, it changed little and decreased to ~0.6 at t=48 h. Figure 5b shows the evolution of $\zeta_{max}/\zeta_{max,0}$ (ζ_{max} is the maximum positive vorticity and $\zeta_{max,0}$ is the initial ζ_{max}) of the different perturbations in the whole field (i.e., not in the 700 km×700 km grid, because the perturbations of some experiments moved outside the grid before t=48 h). All of the $\zeta_{max}/\zeta_{max,0}$ values decreased gradually with diffusion along with the integration. Before t=9 h, the $\zeta_{max}/\zeta_{max,0}$ of SWP had a maximum value followed by that of NP, and that of WP had a the minimum value. However, the $\zeta_{max}/\zeta_{max,0}$ of NP had a maximum value after t=9 h, and it remained at 0.328 at t=48 h, while that of SWP and WP remained at 0.297 and 0.117 at t=48

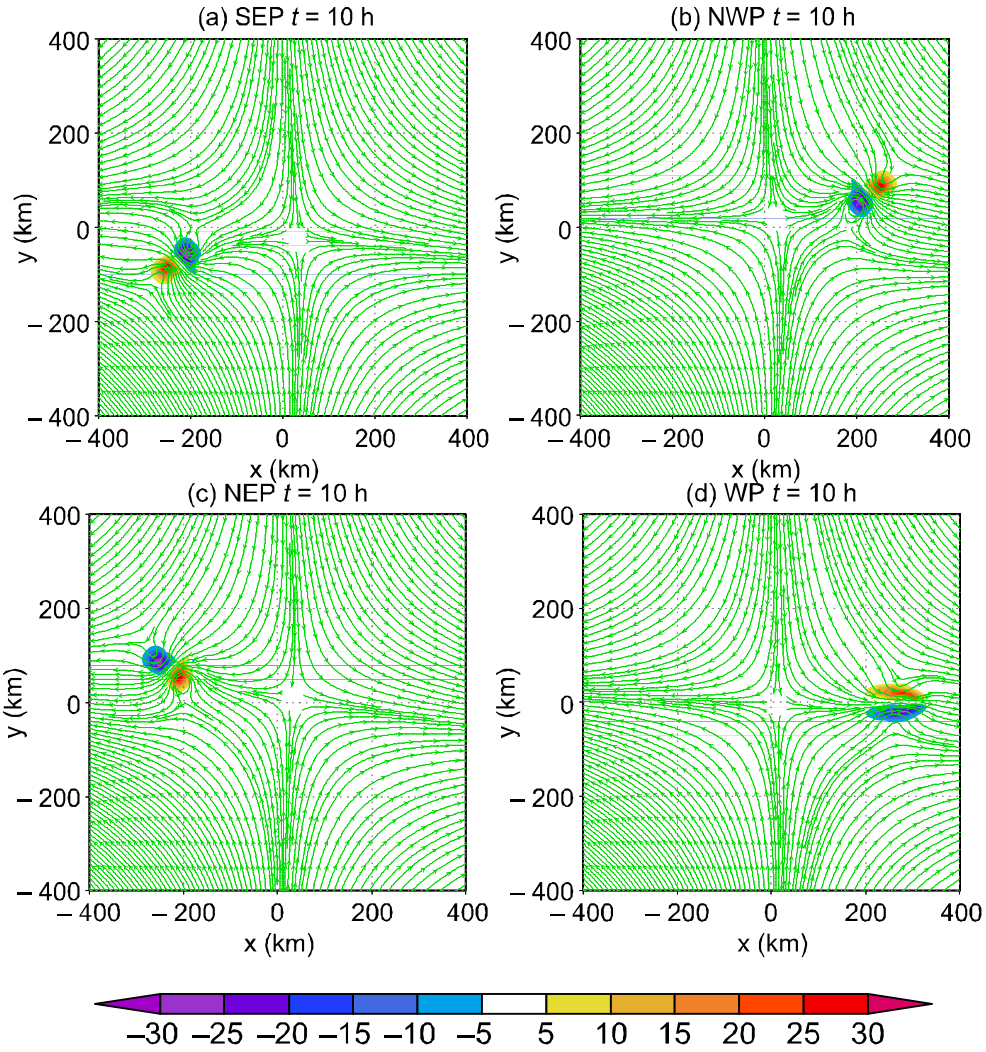

Fig. 4. Simulated stream and vorticity fields induced by (a) SEP, (b) NWP, (c) NEP, and (d) WP at t=10 h. The shadings denote vorticity (units: 10^{-5} s^{-1}).

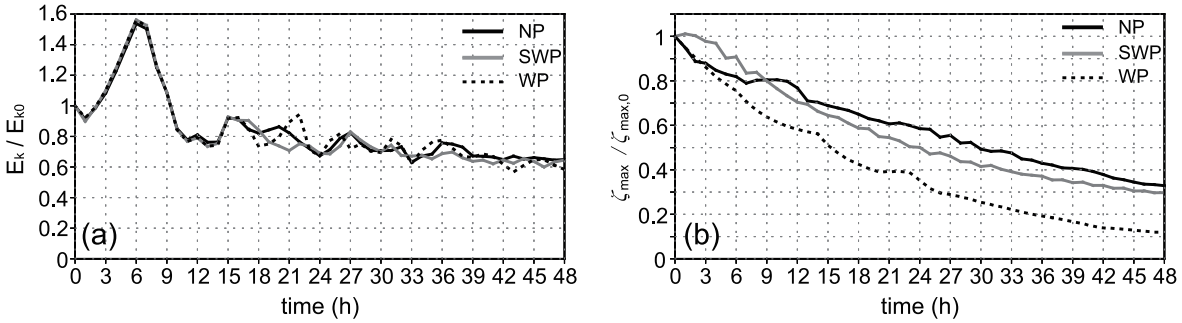

Fig. 5. Evolution of (a) E_k/E_{k0} in the 700 km×700 km grid area and (b) $\zeta_{max}/\zeta_{max,0}$ in the whole field of different perturbations. The black solid lines denote NP, the gray solid lines denote SWP and the dot lines denote WP.

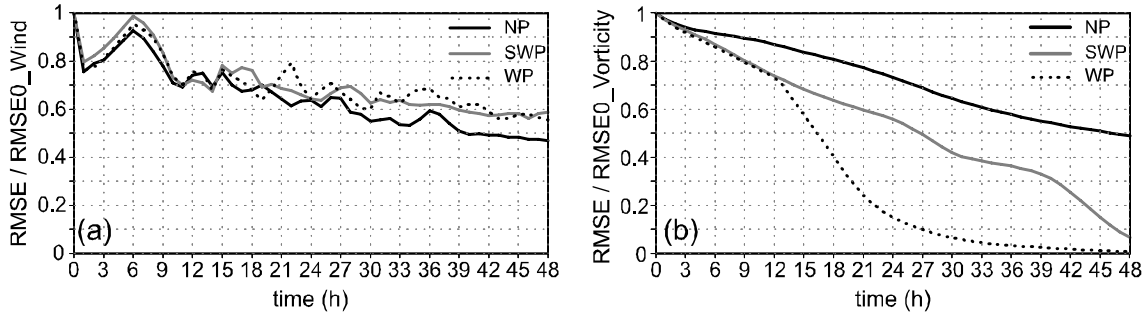

Fig. 6. Evolution of RMSE/RMSE$_0$ of (a) wind speed and (b) vorticity in the 700 km×700 km grid area. The black solid lines denote NP, the gray solid lines denote SWP and the dot lines denote WP.

h, respectively. So the weak environment of the center region of col filed favored the maintenance of the vorticity.

A root mean square error (RMSE) was also utilized to analyze the discrete degree of elements:

$$\mathrm{RMSE} = \sqrt{\frac{1}{N}\sum \left(F_{ij} - F_{\mathrm{A}}\right)^2}, \tag{12}$$

where F is an element, F_{A} is the average of F in the grid area which is the same as the calculation box of E_{k}, and N is the grid number in the grid area.

Figure 6a shows the RMSE/RMSE$_0$ (RMSE$_0$is the initial RMSE) of wind speed. The RMSE/RMSE$_0$ of wind speed of all the perturbations also had a similar tendency like $E_{\mathrm{k}}/E_{\mathrm{k0}}$. The differences of all the perturbations were very small. However, the RMSE/RMSE$_0$ of vorticity of NP, SWP, and WP were distinctly different (Fig. 6b). The RMSE/RMSE$_0$ of vorticity of NP decreased slowly; it remained at 0.87 at t=12 h and at 0.49 at t = 48 h. The RMSE/RMSE$_0$ of vorticity of SWP decreased more rapidly than that of NP; it remained at 0.739 at t = 12 h and decreased to 0.066 at t= 48 h. The RMSE/RMSE$_0$ of vorticity of WP was similar to that of SWP before t=12 h. Because a part of the WP moved outside the 700 km×700 km grid area after t=12 h along the dilatation axis, the RMSE/RMSE$_0$ of vorticity of WP decreased rapidly after t=12 h. This result also indicates the importance of the col field for the maintenance of the perturbation vorticity.

3.5 *Discussion*

These simulations demonstrate that the mesoscale wind perturbations can induce MβV in a weak background. This is confirmed by observations and simulated studies in which the MβVs responsible for heavy rainfalls usually formed in weak wind backgrounds such as col (deformation) fields and shear lines (e.g., Zhang and Fritsch, 1988; Xu and Gao, 2002; Jiang et al., 2004; Long et al., 2006). In this study, the theory that a point vorticity can form a cyclonic (or anticyclonic) circulation (Brown, 1991; Yu et al., 2004) can be used as an explanation.

The intensity of a vorticity source is defined in cylindrical coordinate system as (Brown, 1991)

$$\Gamma = \oint u_\theta \mathrm{d}l = u_\theta 2\pi r, \tag{13}$$

where u_θ is tangential wind speed and $u_\theta = -\partial\psi/\partial r$, and ψ is the stream function. We have the circulation from the line integral around any circle centered at (r, θ)=(0, 0). Equation (13) can be integrated to yield

$$\psi = -\frac{\Gamma}{2\pi}\ln r. \tag{14}$$

In rectangular coordinate system, Eq. (14) can be written as

$$\psi(x,y) = -\frac{\Gamma}{2\pi}\ln\sqrt{(x-x_0)^2+(y-y_0)^2}, \tag{15}$$

where (x_0, y_0) is the location of the point vorticity. If there exists a mesoscale wind perturbation (a WP is taken as an example), there must be two point vorticities at (0, d) and (0, $-d$), respectively (Fig. 7a). Therefore, the stream function can be obtained using

$$\psi(x,y) = -\frac{\Gamma}{2\pi}\ln\sqrt{x^2+(y-d)^2} + \frac{\Gamma}{2\pi}\ln\sqrt{x^2+(y+d)^2}. \tag{16}$$

Therefore, the x-component and y-component of nondivergent wind velocity determined by vorticity can be obtained using

$$u_\psi = \frac{\partial\psi}{\partial y} = \frac{\Gamma}{2\pi}\left[\frac{y+d}{x^2+(y+d)^2} - \frac{y-d}{x^2+(y-d)^2}\right], \tag{17a}$$

$$v_\psi = -\frac{\partial\psi}{\partial x} = \frac{\Gamma}{2\pi}\left[\frac{x}{x^2+(y-d)^2} - \frac{x}{x^2+(y+d)^2}\right]. \tag{17b}$$

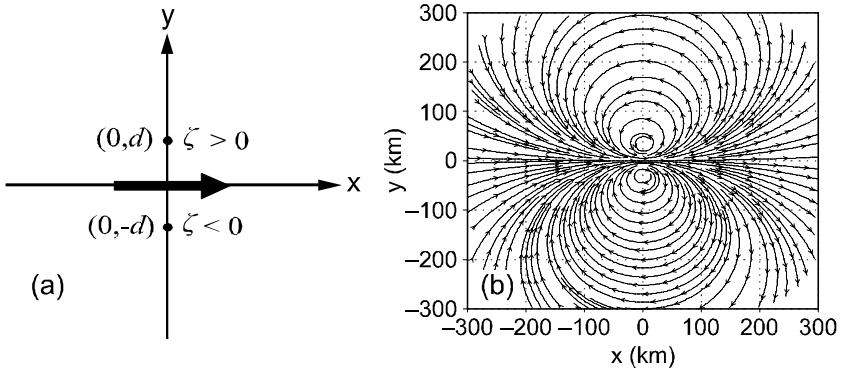

Fig. 7. (a) The sketch map of point vorticity, the heavy arrow denotes the WP, (b) stream field induced by point vorticity.

If d=30 km, the stream field based on Eqs. (17a) and (17b) reveals an MβVC (as shown in Fig. 7b).

Here, the westerly flow and the col field are taken as backgrounds. The background wind velocity is set as 10 m s^{-1} and 2 m s^{-1} as representations of strong and weak backgrounds, respectively, and the intensity of point vorticity is set as $2\pi\times10^5$ m^2 s^{-1}.

Figure 8 shows the superimposed stream fields. When the westerly background is strong with wind velocity of 10 m s^{-1}, there are only curves without any vortex in the field (Fig. 8a), while in the weak wind background with wind velocity of 2 m s^{-1}, there is a very clear MβV (Fig. 8b). However, the vortex in weak westerly flows is so weak that the size of cyclonic circulation is <50 km. When the background is dilatation axis, the size of MβV is ∼80 km (Fig. 8c). Interestingly, the MβV is rather strong as the background field is replaced by a col field in which a cyclonic and an anticyclonic circulations have sizes >100 km (Fig. 8d). The weak wind background favors the formation and development of MβV. In the strong background, the circulation does not develop readily, because the MβV induced by perturbation may be covered up by the strong background flows.

The above analyses considered only the dynamic factors, without taking into account the impact of thermodynamic factors. Because the MβV induced by wind perturbation was relative weak, it could not maintain for long without the thermodynamic effect. In the monsoon season of China, there is often a southwesterly LLJ to the south of col field, which may propagate along the axis of LLJ. The wind velocity fluctuation of the LLJ's core produces a perturbation that tends to move toward the col point or the dilatation axis of col field where the MβV may be easily induced by the perturbation. Furthermore, the LLJ to the south of the col field transports low-level warm and moist air northward, and it produces a convectively unstable layer (Chen, 1983). Once the precipitation is caused by the MβV, the MβV may enhance due to the latent heat release, and then the positive feedback may lead to heavy rainfall. The "98.7" torrential rainfall event was a typical case in which the MβV associated with mLLJ to the south formed in the stable col field (Jiang and Wang, 2010). A numerical simulation of a extremely mei-yu front heavy rainfall event on 4–5 July 2003 also showed that an MβVC associated with an intensified northeasterly flow to the south of mesoscale anticyclone was responsible for the heavy rainfall (Liao and Tan, 2005). That pattern was similar to the case of NEP.

4. A case analysis on the "010805" heavy rainfall event

During 5–6 August 2001, a tropical depression (TD) passed over Shanghai in association with a heavy rainfall. The observed maximum 24-h accumulated precipitation was 275.2 mm in Xujiahui District—a record within the prior 50 years. The TD formed in East China Sea on 3 August and moved westward. After landing on Taiwan Province on 4 August, it turned to the northwest, then turned to the northeast after 1800 UTC 4 August. It passed over Shanghai on the evening of 5 August.

Figure 9 shows the composite 700-hPa flow field from 1 to 9 August 2001, obtained using the digital filter composite method based on Lanczos window function (Hamming, 1989; Lynch and Huang, 1992), with regional spectral model (RSM) 20-km horizontal resolution data from the Japan Meteorological Agency (JMA). The compositing flow field was able to eliminate the irrationally high-frequency noise, and thereby the underlying weather situation was revealed. A col field was located in the vicinity of Taiwan Strait with anticyclonic circulations to the northeast and the west, a trough to the north and an easterly flow to the south.

The TD weakened significantly after landing on

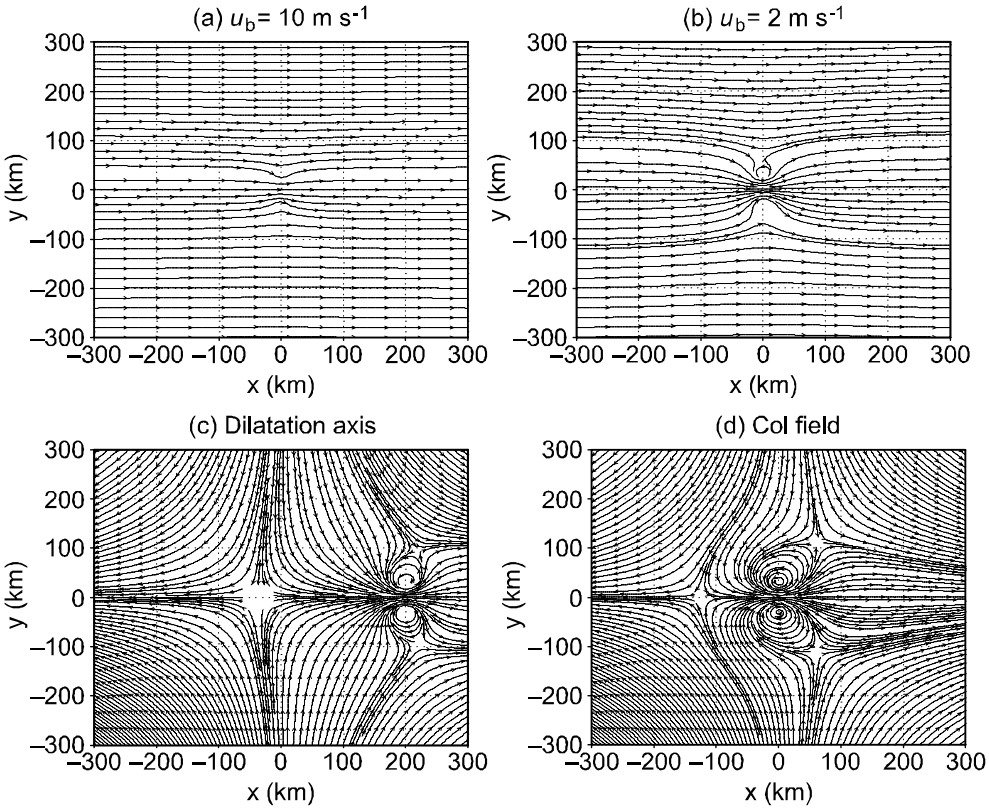

Fig. 8. Stream fields of the wind field induced by point vorticity superimposing on the backgrounds of (a) westerly with wind velocity of 10 m s^{-1}, (b) westerly with wind velocity of 2 m s^{-1}, (c) dilatation axis and (d) col field.

Taiwan in this case. But it enhanced after making landfall on mainland China. To analyze the evolution of the TD as well as the associated LLJs, the transient eddy (TE) of meridional component of wind $v*'$ was calculated using

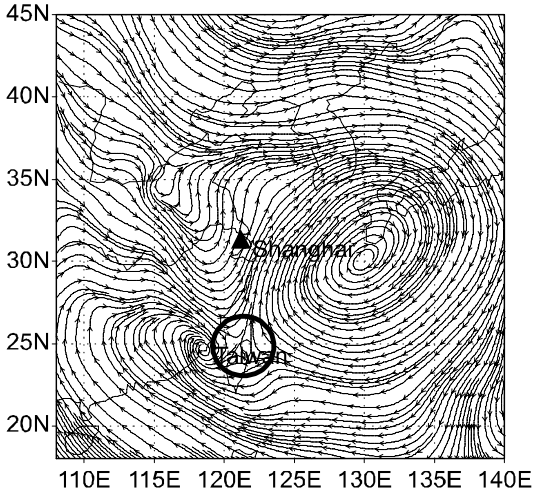

Fig. 9. Composite 700-hPa stream field from 1 to 9 August 2001. The circle and the "▲" denote the location of col field and Shanghai, respectively.

$$v*' = v' - [v'], \tag{18}$$

where $v' = v - \bar{v}$ is the transient wind velocity, v is the meridional component of the wind,

$$\bar{v} = \frac{1}{\tau}\int_0^t v dt\ ,$$

τ is the time range,

$$[v'] = \frac{1}{L}\int_0^L v' dx\ ,$$

and L is the range from 108° to 160°E (the maximum range of the data) in this study.

Figure 10 shows the evolution of the stream, geopotential height and TE of meridional wind. Southerly and northerly TE centers were located to the east and west of the TD, respectively, at 0000 UTC 3 August 2001 (Fig. 10a). The southerly TE was evidently stronger than the northerly TE. The TD moved northwestward and significantly weakened after landing on eastern Taiwan at 1200 UTC 3 August. Although a close isohypse remained, the cyclonic circulation had dissipated (Fig. 10b). The southerly TE to the east of TD was still strong, with the maximum value >12 m s^{-1}. When the TEs entered the col field near the Taiwan Strait (Fig. 9) at 1800 UTC 3 August,

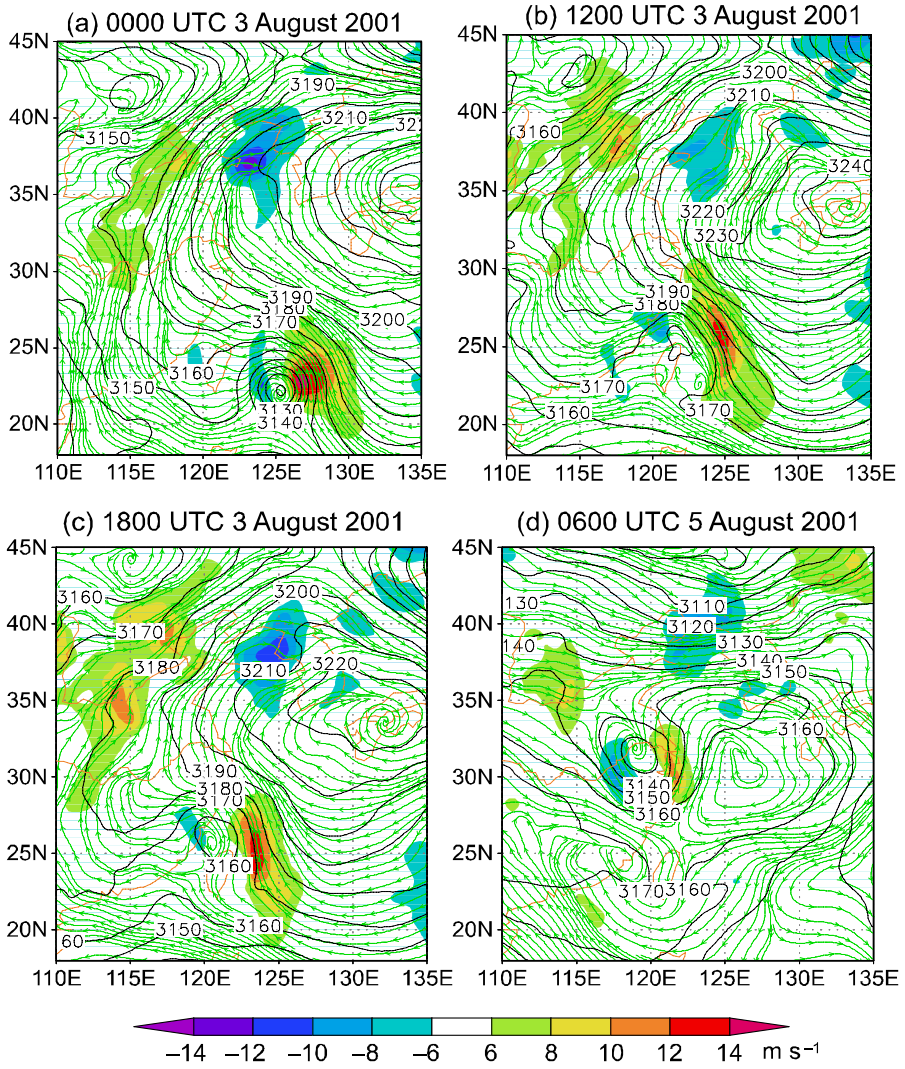

Fig. 10. 700-hPa geopotential height, stream and TE fields at (a) 0000 UTC 3, (b) 1200 UTC 3, (c) 1800 UTC 3, and (d) 0600 UTC 5 August 2001. The solid lines denote the geopotential height (units: gpm), and the shadings denote the TE (units: m s^{-1}) of meridional component of winds.

a meso-β scale cyclonic circulation developed again between the TEs (Fig. 10c). The circulation of the redeveloped TD was enhanced while it moved northward in the col field between the WPSH and the land high.

The TEs rapidly weakened due to the impact of surface friction after landing on the mainland at 0000 UTC 4 August (not shown). The TD moved slowly northward and continued to develop in the col field, while the TEs gradually enhanced. At 0600 UTC 5 August, the maximum TE values to the east and west of the TD increased to 10 and -12 m s^{-1}, respectively (Fig. 10d), and the maximum west TE value further increased to -16 m s^{-1} at 0000 UTC 6 August (not shown). The strengthened TD led to extremely heavy rainfall over Shanghai during this period. The TD was moving so slowly that it spent >2 days crossing the Taiwan Strait, where it redeveloped at 1800 UTC 3 August and proceeded toward the Yangtze River Estuary at 0000 UTC 6 August.

Our analyses of the development and evolution of the TDs show that the redeveloped TD circulation possibly caused by the TEs moved slowly northward and developed continuously. The dynamic effects of TEs and the col field are important for the redevelopment and intensification of the TD. As a background, the flow in the col field was so weak that the TD located near the col point was able to develop rapidly. In this case, the two retainable TEs to the east and west of the

TD, which were similar to the southerly and northerly wind perturbations, played an important role for the redevelopment and enhancement of the TD.

5. Conclusions

The MβVC induced by mesoscale wind perturbation was numerically simulated using a shallow water model in a col field, and the evolution of stream, vorticity, and vortex were analyzed. The formation dynamic mechanism of MβVC induced by wind perturbation can be explained using the theory of point vorticity (e.g., Brown, 1991).

The experiments with eight types of wind perturbations indicate that the development of MβVC was closely related to the location of perturbations. The NP and SP could induce MβVCs, with the sizes of $\sim$100 km. The sizes of MβVCs induced by SWP, SEP, NWP, and NEP were relatively small for the perturbations moving toward the dilatation axis, and the MβVC induced by EP and WP could not develop. The size of the circulation is determined by the distance between the vortex and the col point. The closer to the col point the vortex is, the larger the size of vortex.

The evolution of total kinetic energy per unit mass and the RMSE of wind speed of different perturbations exhibit similar tendencies. However, the maximum vorticity and the RMSE of vorticity of NP decreases slower than that of other perturbations. So the weak environment of the col field favors the maintenance of the vorticity. The results of the simulations also suggest that the stable col field favors the formation and development of the mesoscale vortices. When a mesoscale vortex forms near the col point or moves toward the col point, it may maintain a quasi-stationary state in the stable col field.

Acknowledgements. The authors thank two anonymous reviewers and editors for their valuable comments. This research was supported by the National Fundamental Research Program of China (Grant No. 2009CB421502) and the National Natural Science Foundation of China (Grant Nos. 40830958, 41275099 and 40905021), and the Special Fund for Meteorology-scientific Research in the Public Interest (GYHY200906011). The authors are grateful for the GAME reanalysis data provided by the Japan Meteorological Agency and the Earth Observation Research Center/National Space of Development Agency of Japan.

REFERENCES

Akiyama, T., 1973a: The large-scale aspects of the characteristic features of the Baiu front. *Pap. Meteor. Geophys.*, **24**, 157–188.

Akiyama, T., 1973b: Frequent occurrence of heavy rainfall along the north side to the low-level jet stream in the Baiu season. *Pap. Meteor. Geophys.*, **24**, 379–388.

Arritt, R. W., T. D. Rink, M. Segal, D. P. Todey, C. A. Clark, M. J. Mitchell, and K. M. Labas, 1997: The Great Plains low-level jet during the warm season of 1993. *Mon. Wea. Rev.*, **125**, 2176–2192.

Bartels, D. L., and R. A. Maddox, 1991: Midlevel cyclonic vortices generated by mesoscale convective systems. *Mon. Wea. Rev.*, **119**, 104–118.

Bei, N. F., S. X. Zhao, and S. T. Gao, 2002: Numerical simulation of a heavy rainfall event in China during July 1998. *Meteor. Atmos. Phys.*, **80**, 153–164.

Brown, R. A. 1991: *Fluid Mechanics of the Atmosphere*. Academic Press, Inc., 489pp.

Chen, D., Y. Q. Li, and R. H. Huang, 2007: The physical process analyses of the southwest vortex development and its effect on heavy rainfall in Eastern Sichuan under the saddle pattern background of large-scale circulations. *Chinese J. Atmos. Sci.*, **31**(2), 185–201. (in Chinese with English abstract)

Chen, L. S., and W. H. Feng, 2003: Structural evolution of the genesis and development on meso-β vortex for the "98.7" heavy rainfall: Simulation of two ways with quartet nested grid. *Acta Meteorologica Sinica*, **61**(4), 385–395. (in Chinese with English abstract)

Chen, G. T. J., 1983: Observational aspects of the Meiyu phenomena in subtropical China. *J. Meteor. Soc. Japan*, **61**, 306–312.

Chen, G. T. J., and C. C. Yu, 1988: Study of low-level jet and extremely heavy rainfall over northern Taiwan in the Mei-yu season. *Mon. Wea. Rev.*, **116**, 884–891.

Chen, G. T. J., and Y. S. Hsu, 1997: Composite structure of a low-level jet over southern China observed during the TAMEX period. *J. Meteor. Soc. Japan*, **75**, 1003–1018.

Chen, G. T. J., C. C. Wang, and D. T. W. Lin, 2005: Characteristics of low-level jets over northern Taiwan in Mei-yu season and their relationship to heavy rain events. *Mon. Wea. Rev.*, **133**, 20–43.

Chen, G. T. J., C. C. Wang, and L. F. Lin, 2006: A diagnostic study of a retreating Mei-yu front and the accompanying low-level jet formation and intensification. *Mon. Wea. Rev.*, **134**, 874–896.

Chen, Q. S., 1982: The instability of the gravity-inertia wave and its relation to low-level jet and heavy rain. *J. Meteor. Soc. Japan*, **60**, 1041–1057.

Chen, S. J., Y. H. Kuo, W. Wang, Z. Y. Tao, and B. Cui, 1998: A modeling case study of heavy rainstorms along the Mei-yu front. *Mon. Wea. Rev.*, **126**, 2330–2351.

Chen, S. S., and W. M. Frank, 1993: A numerical study of the genesis of extratropical convective mesovortices, Part I: Evolution and dynamics. *J. Atmos. Sci.*, **50**, 2401–2426.

Chu, K. K., and Z. M. Tan, 2010: Mesoscale moist adjoint sensitivity study of a Mei-yu heavy rainfall event. *Adv. Atmos. Sci.*, **27**(6), 1415–1424, doi:

10.1007/s00376-010-9213-1.

Davis, C. A., and M. L. Weisman, 1994: Balanced dynamics of mesoscale vortices produced in simulated convective systems. *J. Atmos. Sci.*, **51**, 2005–2030.

Erbes, G., 1992: A high-resolution Lax-Friedrichs scheme for hyperbolic conservation laws with source terms: Application to shallow water equations. Tech. Rep. 62, Department of Meteorology, Stockholm University, 49pp.

Erbes, G., 1993: A semi-Lagrangian method of characteristic for the shallow-water equations. *Mon. Wea. Rev.*, **121**, 3443–3452.

Fritsch, J. M., J. D. Murphy, and J. S. Kain, 1994: Warm core vortex amplification over land. *J. Atmos. Sci.*, **51**, 1780–1807.

Hamming, R. W., 1989: *Digital Filters*. 3rd ed., Prentice-Hall, Englewood Cliffs, New Jersey, 284pp.

Hertenstein, R. F. A., and W. H. Schubert, 1991: Potential vorticity anomalies associated with squall lines. *Mon. Wea. Rev.*, **119**, 1663–1672.

Houze, R. A., Jr., 2004: Mesoscale convective systems. *Rev. Geophys.*, **42**, RG4003, doi: 10.1029/2004RG000150.

Hu, B. W., C. G. Cui, and C. H. Fang. 2001: Causes of a two-day successively extremely heavy rain along the Changjiang valley in the eastern Hubei Province during 21–22 July 1998. *Chinese J. Atmos. Sci.*, **25**(4), 479–491. (in Chinese with English abstract)

Jiang, H., and D. J. Raymond, 1995: Simulation of a mature mesoscale convective system using a nonlinear balance model. *J. Atmos. Sci.*, **52**, 161–175.

Jiang, Y. Q., and Y. Wang. 2010: Effects of terrain on saddle pattern during the course of "98.7" extremely heavy rainstorm in the East of Hubei Province. *Plateau Meteorology*, **29**(2), 298–308. (in Chinese with English abstract)

Jiang, Y. Q., C. Y. Wang, W. H. Zhang, and Z. Y. Chen, 2004: Numerical simulation of extremely heavy rain and meso-β scale low vortex in inverted typhoon trough. *Acta Meteorologica Sinica*, **18**(2), 195–210.

Johnston, E. C., 1981: Mesoscale vorticity centers induced by mesoscale convective complexes. M.S. thesis, Dept. of Atmospheric and Oceanic Sciences, University of Wisconsin, 54pp.

Li, J., Y. L. Chen, and W. C. Lee, 1997: Analysis of a heavy rainfall event during TAMEX. *Mon. Wea. Rev.*, **125**, 1060–1081.

Liao, J., and Z. M. Tan, 2005: Numerical simulation of a heavy rainfall event along the Meiyu front: Influences of different scale weather systems. *Acta Meteorologica Sinica*, **63**(5), 771–789. (in Chinese with English abstract)

Long, X., L. S. Chen, and L. J. Wen, 2006: A numerical study of the structure and evolution of meso-β scale system during "02.6" Meiyu. *Chinese J. Atmos. Sci.*, **30**(2), 327–340. (in Chinese with English abstract)

Lynch, P., and X. Y. Huang, 1992: Initialization of the HIRLAM model using a digital filter. *Mon. Wea. Rev.*, **120**, 1019–1034.

Matsumoto, S., 1973: Lower tropospheric wind speed and precipitation activity. *J. Meteor. Soc. Japan*, **51**, 101–107.

Ninomiya, K., and T. Akiyama, 1974: Band structure of mesoscale echo clusters associated with low-level jet stream. *J. Meteor. Soc. Japan*, **52**, 300–313.

Petterssen, S., 1956: *Motion and Motion Systems*. Vol. I, *Weather Analysis and Forecasting*, 2nd ed., McGraw-Hill, 428pp.

Ray, P. S., 1986: *Mesoscale Meteorology and Forecasting*. Amer. Meteor. Soc., 793pp.

Raymond, D. J., and H. Jiang, 1990: A theory for long-lived mesoscale convective systems. *J. Atmos. Sci.*, **47**, 3067–3077.

Rutledge, S. A., and R. A. Houze Jr., 1987: A diagnostic modeling study of the trailing stratiform region of a midlatitude squall line. *J. Atmos. Sci.*, **44**, 2640–2656.

Sun, J. H., S. X. Zhao, G. K. Xu, and Q. T. Meng, 2010: Study on a mesoscale convective vortex causing heavy rainfall during the Mei-yu season in 2003. *Adv. Atmos. Sci.*, **27**(5), 1193–1209, doi: 10.1007/s00376-009-9156-6.

Tao, S. Y., 1980: *The Torrential Rain in China*. Science Press, Beijing, 225pp. (in Chinese)

Wang, Z., and K. Gao, 2006: Adjoint sensitivity experiments of a meso-β-scale vortex in the middle reaches of the Yangtze River. *Adv. Atmos. Sci.*, **23**(2), 267–281, doi: 10.1007/s00376-006-0267-z.

Xu, W. H., Y. Q. Ni, X. K. Wang, X. X. Qiu, X. H. Bao, and W. Y. Jin, 2011: A study of structure and mechanism of a meso-beta-scale convective vortex and associated heavy rainfall in the Dabie Mountain area Part I: Diagnostic analysis of the structure. *Adv. Atmos. Sci.*, **28**(5), 1159–1176, doi: 10.1007/s00376-010-0170-5.

Xu, Y. M., and K. Gao. 2002: Simulation and analysis of meso-β vortex over middle reaches of the Yangtse River on 22 July 1998. *Acta Meteorologica Sinica*, **60**(1), 85–95. (in Chinese with English abstract)

Yu, Z. H., M. Q. Miao, Q. R. Jiang, and P. Z. Yang, 2004: *Hydrodynamics*. China Meteorological Press, Beijing, 378pp. (in Chinese)

Zhai, G. Q., L. L. Zhou, and Z. Wang, 2007: Analysis of a group of weak small-scale vortexes in the planetary boundary layer in the Mei-yu front. *Adv. Atmos. Sci.*, **24**(3), 399–408, doi: 10.1007/s00376-007-0399-9.

Zhang, D. L., and J. M. Fritsch, 1988: A numerical investigation of a convectively generated, inertially stable, extratropical warm-core mesovortex over land. Part I: Structure and evolution. *Mon. Wea. Rev.*, **116**, 2660–2687.